Science
AAAS

Human-Induced Arctic Moistening
Seung-Ki Min, *et al.*
Science **320**, 518 (2008);
DOI: 10.1126/science.1153468

Science (print ISSN 0036-8075; online ISSN 1095-9203) is published weekly, except the last week in December, by the American Association for the Advancement of Science, 1200 New York Avenue NW, Washington, DC 20005.

Human-Induced Arctic Moistening

Seung-Ki Min, Xuebin Zhang, Francis Zwiers*

The Arctic and northern subpolar regions are critical for climate change. Ice-albedo feedback amplifies warming in the Arctic, and fluctuations of regional fresh water inflow to the Arctic Ocean modulate the deep ocean circulation and thus exert a strong global influence. By comparing observations to simulations from 22 coupled climate models, we find influence from anthropogenic greenhouse gases and sulfate aerosols in the space-time pattern of precipitation change over high-latitude land areas north of 55°N during the second half of the 20th century. The human-induced Arctic moistening is consistent with observed increases in Arctic river discharge and freshening of Arctic water masses. This result provides new evidence that human activity has contributed to Arctic hydrological change.

Arctic and northern subpolar regions play a key role in determining the effects of human-induced forcing of the climate system and are expected to be affected more strongly than other regions. Polar amplification due to meridional heat transport and positive ice-albedo feedback results in more rapid warming at high latitudes than at lower latitudes. Arctic ecosystems, which are very vulnerable to environmental changes, are experiencing the impacts of climate change sooner and more strongly than elsewhere (*1*–*3*). Freshwater inflow into the Arctic Ocean is a critical factor in determining ocean convection in the subarctic seas, affecting the Atlantic Ocean meridional overturning circulation (MOC) and thus the global climate (*4*, *5*).

Observational studies show that precipitation and river discharge have increased in the Arctic region during the past 50 years, together with ocean freshening (*3*, *5*–*7*). Most recent global climate models (GCMs) project northern high-latitude precipitation increases and MOC weakening in the future (*8*). Nevertheless, the question of whether humans have contributed to the observed Arctic precipitation increase has, until now, remained unanswered.

Human influence on the climate has been detected in surface temperature at global and regional scales and in free atmospheric temperature, tropopause height, sea level pressure, ocean heat content, and surface and atmospheric humidity at global scales (*9*–*11*). Detecting preciptation response to external forcing is more challenging for several reasons: The signal-to-noise ratio is lower, global precipitation changes may be constrained by changes in the atmospheric energy balance that results in a smaller precipitation change per unit climate forcing from greenhouse gases than from other agents (*9*, *12*), and the local nature of precipitation makes it more difficult to develop spatiotemporally complete data sets (*12*). Nevertheless, the effects of external forcing on global land precipitation totals (*13*–*15*) and of anthropogenic forcing on the zonal distribution of global land precipitation (*16*) have been detected in observations. Here, we demonstrate a detectable anthropogenic influence on the observed change in Arctic land precipitation over the latter half of the 20th century.

Many Arctic watersheds extend farther south than the area that is traditionally considered as the Arctic region (*3*). The Canadian and Eurasian Arctic flowing watersheds in particular extend to south of 50°N. For the purpose of this analysis, we consider latitude 55°N as the southern boundary for the Arctic. This includes most of the Arctic-flowing river basins in both North America and Eurasia while excluding regions with mid-latitude climate regimes as much as possible.

We used monthly precipitation amounts from the Global Historical Climatology Network (GHCN) data set (*17*), compiled and quality controlled at the National Oceanic and Atmospheric Administration's National Climatic Data Center. Because the availability of station data is limited before 1950, we restricted ourselves to the time period from 1950 to 1999. Canadian stations in the GHCN have many missing values in the 1990s. We therefore replaced Canadian data in the GHCN with 495 adjusted precipitation records (*18*). The resulting combined pan-Arctic data set has reasonably good spatial and temporal coverage and benefits from adjustments for many known precipitation measurement issues (*18*). Nevertheless, uncertainty remains because of the difficulty in measuring precipitation in this region. Monthly precipitation anomalies relative to 1961 to 1990 were subsequently calculated and gridded at the 5° × 5° latitude-longitude resolution before the analyses (*18*).

We used climate simulations obtained from the Coupled Model Intercomparison Project phase 3 (CMIP3) archive and directly from modeling centers. They included ANT simula-

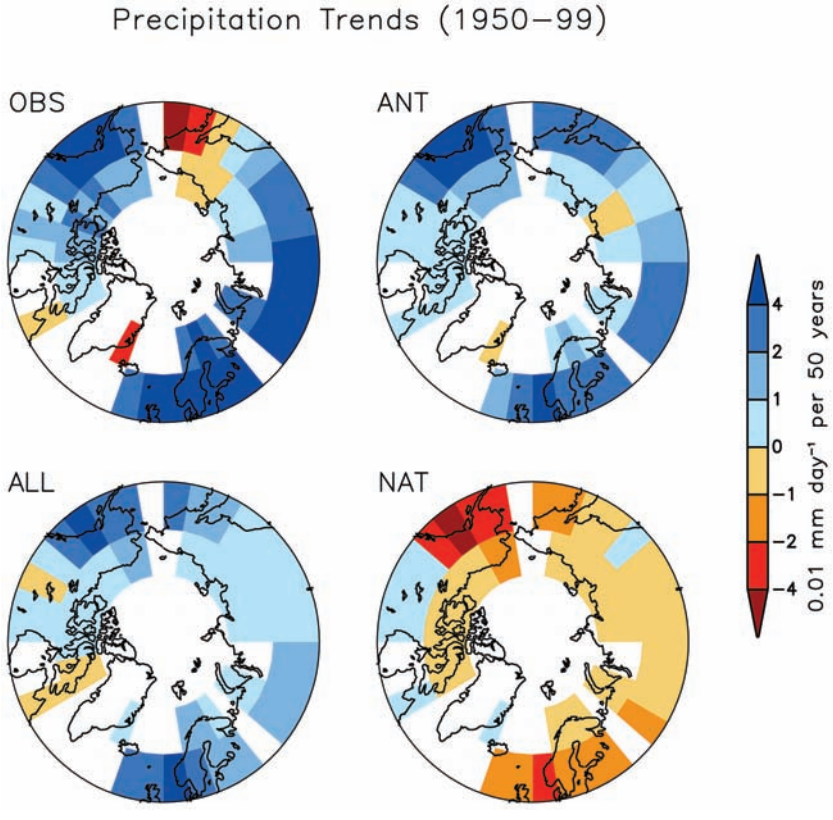

Fig. 1. Large-scale precipitation trends (0.01 mm day^{-1} per 100 years) during 1950 to 1999 from the observations (OBS) and ALL, ANT, and NAT simulations. Large-scale precipitation variation is represented by the first five spatial EOFs of 5-year mean precipitation from the CTL simulations (*18*). Areas with less than 40 years of observations are marked with white space.

Climate Research Division, Environment Canada, Toronto, Ontario M3H 5T4, Canada.

*To whom correspondence should be addressed. E-mail: Francis.Zwiers@ec.gc.ca

tions with historical anthropogenic forcing from greenhouse gases and sulfate aerosols, NAT simulations with reconstructed natural (volcanic and solar) external forcing, and ALL simulations with both anthropogenic and natural external forcing. Control (CTL) simulations were also used when estimating the natural internal variability of precipitation. Details of each group are summarized in table S1. All simulations were interpolated to the same 5° × 5° grid as used for the observations and were masked to mimic the availability of the observational data (*18*).

We used the five leading spatial EOFs (empirical orthogonal functions) computed from the 5-year mean precipitation fields of the multimodel CTL simulations (*18*) to represent the large-scale precipitation variation in the region. These EOFs account for 52% of the total CTL simulation variability of 5-year mean precipitation. We projected 5-year mean precipitation anomalies from the observations and from the ALL, ANT, and NAT simulations onto those EOFs.

Figure 1 shows the large-scale precipitation trends during 1950 to 1999. The observed change is characterized by an overall increasing trend together with a decreasing trend over the easternmost part of Eurasia, as has been previously reported (*3*, *6*, *16*, *19*). The overall multimodel mean trend under ANT forcing resembles that which is observed, but with smaller amplitude. It is also consistent with projected future precipitation change under much stronger greenhouse warming (*8*). The ALL trend has a pattern very similar to the ANT trend, whereas the NAT trend exhibits a pattern of opposite sign.

We compared the observed and simulated space-time variation of precipitation (composed of ten 5-year means, each represented in the five EOF space) using the standard optimal detection approach (*20*–*22*). This method expresses the observations ($\mathbf{y}$) as a sum of scaled response patterns or "fingerprints" ($\mathbf{X}$) estimated from forced GCM simulations plus internal variability ($\boldsymbol{\varepsilon}$): $\mathbf{y} = \mathbf{X}\boldsymbol{\beta} + \boldsymbol{\varepsilon}$. We regressed the observations onto the multimodel mean ALL, ANT, and NAT patterns separately to identify observed precipitation responses to individual forcing factors ("one-signal analysis"). To examine the relative contribution of natural and anthropogenic forcings to the observed precipitation variation, we also conducted a "two-signal analysis" by regressing observations onto the ANT and NAT patterns simultaneously (*20*). These regressions scale the model-simulated fingerprints to best fit the observations. The scaling factors $\boldsymbol{\beta}$ were estimated using the total least squares method (*21*) so as to account for sampling errors in the model-simulated fingerprints.

The two independent estimates of internal variability needed in the estimation and testing of the scaling factors were obtained using both forced and unforced multimodel simulations. Only the multimodel mean values for ALL, ANT, NAT, and CTL simulations respectively were removed from the runs that make up these ensembles when estimating the space-time internal variability covariance matrices, thereby accounting for intermodel variability in the forced response (*18*). Our detection analyses were conducted in a space spanned by the first 14 space-time EOFs of the first of the two 50-dimensional covariance matrices (five principal components for each of ten 5-year periods) obtained in this way. Our detection results are insensitive to reasonable variations in the number of space-time EOFs, as are the results of the residual consistency test (*22*) that was used to compare simulated and observed internal variability. Detection of the response to external forcing is claimed when the 5 to 95% range of the scaling factors $\boldsymbol{\beta}$ lies above zero. The robustness of the detection results is also examined by inflating estimated internal variability by a factor of two.

Figure 2A shows the one-dimensional scaling factors and their 90% confidence ranges estimated with and without doubling model-estimated internal variability. ANT is clearly detected in the one-signal analysis. Although ALL is also robustly detected, NAT is not detectable. The two-signal analysis results indicate that the Arctic precipitation response to ANT forcing can be separated from that of NAT and that the response to ALL forcing in the observations is a manifestation of the response to ANT forcing (also see fig. S1). A two-signal analysis that uses ANT and NAT simulations from the same group of the models produced similar results (fig. S2 and supporting online text). The temporal evolution of the spatial patterns of precipitation change in both observations and simulations (fig. S3) shows similar zonal variations, suggesting that these zonal variations are important contributors to our Arctic domain detection result, just as meridional variation between zonal means is key to detection on the global scale (*16*). Detection results using Arctic average precipitation are less robust (fig. S4). However, detection analyses of precipitation averaged meridionally over three large subregions of the Arctic to retain only very large scale zonal variation in land precipitation yield results similar to those from the full analysis, which underscores the importance of considering the zonal pattern of Arctic precipitation change in the detection analysis (fig. S4 and supporting online text).

It should be noted that for the ANT response, the 5 to 95% scaling factor range lies above 1, with a best-guess value of about 3 (Fig. 2A), suggesting that the multimodel ensemble Arctic precipitation response to ANT

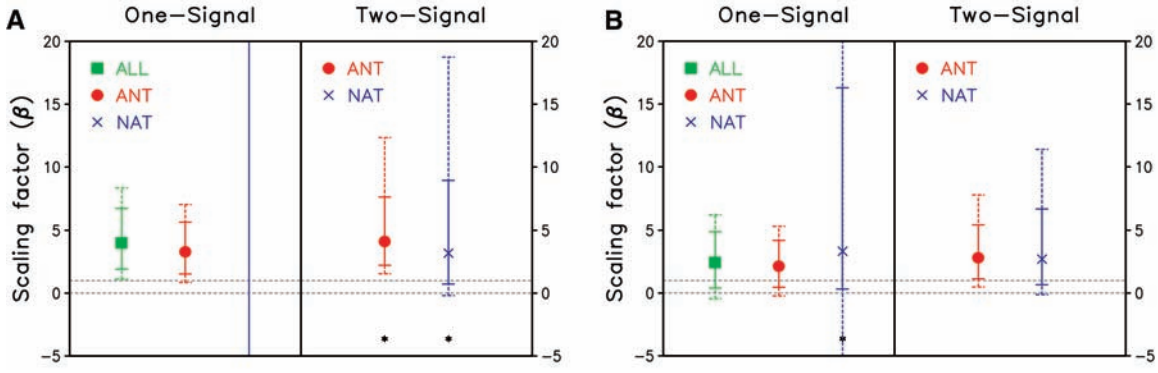

Fig. 2. Best estimates of the scaling factors and their 5 to 95% uncertainty ranges from one-signal and two-signal space-time analyses of 1950 to 1999 Arctic precipitation anomalies with (**A**) raw observations and (**B**) observations from which AO-related variability has been removed. In the one-signal analysis, observed precipitation anomalies are separately regressed onto the multimodel mean precipitation anomalies of all available ALL, ANT, and NAT simulations, respectively. In the two-signal analysis, observed precipitation anomalies are regressed onto the multimodel mean precipitation anomalies from ANT and NAT simulations simultaneously. The first 14 space-time EOFs have been retained in the optimal detection analysis, which explains 55% of total internal variance of the 50-dimensional analysis vector (five principal components for ten 5-year periods). Dashed error bars represent the estimated uncertainty range when model-simulated variability is doubled. The asterisks (*) indicate that the residual consistency test (*22*) is passed only if model-simulated variability is doubled.

forcing is generally underestimated. This is consistent with other studies indicating that models undersimulate precipitation responses to external forcing (*13*–*16*, *23*).

The Arctic Oscillation (AO) is an important contributor to Northern Hemisphere climate variability (*1*, *3*). The prolonged positive AO phase during recent decades is in accord with precipitation changes over Europe and the Arctic (*3*, *24*, *25*). Although modeled AO responses to anthropogenic forcing are generally weaker than observed (*26*, *27*), some studies suggest anthropogenic influences may have been a factor (*9*). To test the sensitivity of our detection results to the possible effect of AO fluctuations, we repeated our detection analyses on observed precipitation series that exclude variability linearly related to the AO. We did so by linearly regressing the observed gridded monthly precipitation anomalies onto the AO index, defined as the first principal component of the monthly mean sea level pressure anomalies north of 20°N (*25*) and by retaining only the regression residuals for detection analyses. The detection results obtained in this way (Fig. 2B) are improved: The scaling factors are closer to one, and model-simulated variability agrees better with observed. This increases confidence in our detection result because it demonstrates human influence on aspects of Arctic precipitation change that are not related to a component of circulation change that has been associated with model structural uncertainty. Nevertheless, it remains difficult to assess the effects of model structural uncertainty, as well as that of observational uncertainty, on our results.

Our results indicate that anthropogenic forcing from greenhouse gases and sulfate aerosols combined has contributed to the observed high-latitude precipitation increase during the latter half of the 20th century. We also find that model-simulated precipitation responses to anthropogenic forcing are weaker than in the observations. This implies that model-projected future precipitation change may also be too weak, which would have important implications for the development of adaptation strategies: It is possible that future Arctic Ocean freshening and MOC slowdown could occur more quickly than indicated by currently available GCM simulations (*7*). Recent studies show that Arctic sea ice is declining substantially faster than indicated by model simulations (*28*, *29*).

References and Notes

1. R. E. Moritz, C. M. Bitz, E. J. Steig, *Science* **297**, 1497 (2002).
2. IPCC, *Climate Change 2007: Impacts, Adaptation and Vulnerability. Contribution of Working Group II to the Fourth Assessment Report of IPCC* (Cambridge Univ. Press, Cambridge, 2007).
3. ACIA, *Arctic Climate Impact Assessment: Scientific Report* (Cambridge Univ. Press, Cambridge, 2005).
4. S. Rahmstorf, *Nature* **419**, 207 (2002).
5. B. J. Peterson *et al.*, *Science* **298**, 2171 (2002).
6. K. E. Trenberth *et al.*, in *Climate Change 2007: The Physical Science Basis. Contribution of Working Group I to the Fourth Assessment Report of IPCC*, (Cambridge Univ. Press, Cambridge, 2007), pp. 235–336.
7. B. J. Peterson *et al.*, *Science* **313**, 1061 (2006).
8. G. A. Meehl *et al.*, in *Climate Change 2007: The Physical Science Basis. Contribution of Working Group I to the Fourth Assessment Report of IPCC* (Cambridge Univ. Press, Cambridge, 2007), pp. 747–845.
9. G. C. Hegerl *et al.*, in *Climate Change 2007: The Physical Science Basis. Contribution of Working Group I to the Fourth Assessment Report of IPCC* (Cambridge Univ. Press, Cambridge, 2007), pp. 663–745.
10. K. M. Willett, N. P. Gillett, P. D. Jones, P. W. Thorne, *Nature* **449**, 710 (2007).
11. B. D. Santer *et al.*, *Proc. Natl. Acad. Sci. U.S.A.* **104**, 15248 (2007).
12. M. R. Allen, W. J. Ingram, *Nature* **419**, 224 (2002).
13. F. H. Lambert, P. A. Stott, M. R. Allen, M. A. Palmer, *Geophys. Res. Lett.* **31**, 10203 (2004).
14. N. P. Gillett, A. J. Weaver, F. W. Zwiers, M. F. Wehner, *Geophys. Res. Lett.* **31**, 12217 (2004).
15. F. H. Lambert, N. P. Gillett, D. A. Stone, C. Huntingford, *Geophys. Res. Lett.* **32**, 18704 (2005).
16. X. Zhang *et al.*, *Nature* **448**, 461 (2007).
17. T. C. Peterson, R. S. Vose, *Bull. Am. Meteorol. Soc.* **78**, 2837 (1997).
18. Materials and methods are available as supporting material on *Science* Online.
19. G. Gruza, E. Rankova, V. Razuvaev, O. Bulygina, *Clim. Change* **42**, 219 (1999).
20. G. C. Hegerl *et al.*, *Clim. Dyn.* **13**, 613 (1997).
21. M. R. Allen, P. A. Stott, *Clim. Dyn.* **21**, 477 (2003).
22. M. R. Allen, S. F. B. Tett, *Clim. Dyn.* **15**, 419 (1999).
23. F. J. Wentz, L. Ricciardulli, K. Hilburn, C. Mears, *Science* **317**, 233 (2007).
24. D. W. J. Thompson, J. M. Wallace, *Science* **293**, 85 (2001).
25. D. W. J. Thompson, J. M. Wallace, G. C. Hegerl, *J. Clim.* **13**, 1018 (2000).
26. N. P. Gillett, *Nature* **437**, 496 (2005).
27. R. L. Miller, G. A. Schmidt, D. T. Shindell, *J. Geophys. Res.* **111**, D18101 (2006).
28. M. C. Serreze, M. M. Holland, J. Stroeve, *Science* **315**, 1533 (2007).
29. J. Stroeve, M. M. Holland, W. Meier, T. Scambos, M. Serreze, *Geophys. Res. Lett.* **34**, L09501 (2007).

30. We thank R. Vose and P. Ya. Groisman at the National Climatic Data Centre for the observed precipitation data, and P. Stott and T. Nozawa for the provision of model data. We are grateful to M. Mackay, W. Skinner, and two anonymous reviewers for their helpful comments. We acknowledge the modeling groups, the Program for Climate Model Diagnosis and Intercomparison (PCMDI), and the World Climate Research Programme's (WCRP) Working Group on Coupled Modelling (WGCM) for their roles in making available the WCRP CMIP3 multimodel data set. Support of this data set is provided by the Office of Science, U.S. Department of Energy. S.-K.M. is supported by the Canadian International Polar Year program.

Supporting Online Material

www.sciencemag.org/cgi/content/full/320/5875/518/DC1
Materials and Methods
SOM Text
Figs. S1 to S4
Tables S1 and S2
References

27 November 2007; accepted 18 March 2008
10.1126/science.1153468

Efficient Inhibition of the Alzheimer's Disease β-Secretase by Membrane Targeting

Lawrence Rajendran,[1] Anja Schneider,[2] Georg Schlechtingen,[3,4] Sebastian Weidlich,[4] Jonas Ries,[5] Tobias Braxmeier,[3,4] Petra Schwille,[5] Jörg B. Schulz,[6] Cornelia Schroeder,[4] Mikael Simons,[2] Gary Jennings,[3] Hans-Joachim Knölker,[3,4] Kai Simons[1]*

β-Secretase plays a critical role in β-amyloid formation and thus provides a therapeutic target for Alzheimer's disease. Inhibitor design has usually focused on active-site binding, neglecting the subcellular localization of active enzyme. We have addressed this issue by synthesizing a membrane-anchored version of a β-secretase transition-state inhibitor by linking it to a sterol moiety. Thus, we targeted the inhibitor to active β-secretase found in endosomes and also reduced the dimensionality of the inhibitor, increasing its local membrane concentration. This inhibitor reduced enzyme activity much more efficiently than did the free inhibitor in cultured cells and in vivo. In addition to effectively targeting β-secretase, this strategy could also be used in designing potent drugs against other membrane protein targets.

A key molecule in the pathogenesis of Alzheimer's disease (AD) is the β-amyloid peptide (Aβ), which, either in its soluble oligomeric form or in the plaque-associated version, leads to neurodegeneration (*1*). Aβ is liberated from the membrane-spanning β-amyloid precursor protein (APP) by sequential proteolytic processing using β- and γ-secretases. β-Secretase activity is conferred by a transmembrane aspartyl protease, also termed BACE-1 (β-amyloid cleaving enzyme 1), which catalyzes the rate-limiting reaction in the generation of Aβ (*2*). β-Secretase cleavage of APP occurs predominantly in endosomes, and endocytosis of APP and β-secretase is essential for β cleavage and Aβ production (*3*–*7*). The low pH of endosomes is optimal for β-secretase activity. Conversely, α-secretase cleavage of APP, which precludes production of the toxic Aβ peptide, occurs at the plasma membrane (*8*). Both β- and γ-secretase are thus propitious therapeutic targets (*1*, *9*). However, in